大橋 秀伯・伊藤 大知・山口 猛央
高分子中の分子拡散性を予測するミクロな新規自由体積モデルの構築
１７）International Symposium on Engineering Micro-/Nano-Materials based on Self-Assembling and Self-Organization, ISEM2008 Returns
The National Museum of Emerging Science and Innovation (Miraikan), Japan
Dec. 8-10, 2008
No.8
Hidenori Kuroki, Hidenori Ohashi, Taichi Ito and Takeo Yamaguchi
Development of Novel Bioresponsive Gating System using Biorecognition Crosslinker
１８）膜シンポジウム 2008
大阪大学豊中キャンパス
2008 年 11 月 14 日 -15 日
111
伊藤 大知・大橋 秀伯・山口 猛央
Nonlinear Self-Excited Oscillation of a Synthetic Ion Channel-Inspired Membrane
１９）膜シンポジウム 2008
大阪大学豊中キャンパス
2008 年 11 月 14 日 -15 日
215
大橋 秀伯・伊藤 大知・山口 猛央
ミクロな自由体積理論を用いた高分子中の分子拡散性予測：気体・溶媒から溶質分子まで
２０）日韓高分子若手シンポジウム発表 (JAPAN-KOREA Polymer Young Scientist Symposium)
Niigata
October 23-25, 2008
F22
Ju-Myeung Lee, Hidenori Ohashi, Taichi Ito, Takeo Yamaguchi,
Capping Phenomenon on Interface Between Nanoparticles and Electrolyte Polymer and Its Application to Polymer Electrolyte Fuel Cells
２１）日韓高分子若手シンポジウム発表 (JAPAN-KOREA Polymer Young Scientist Symposium)
Niigata
October 23-25, 2008
F24
Taichi Ito, Hidenori Ohashi, Takeo Yamaguchi
Nonlinear Self-Excited Oscillation of a Synthetic Ion Channel-Inspired Membrane
２２）日韓高分子若手シンポジウム発表 (JAPAN-KOREA Polymer Young Scientist Symposium)
Niigata
October 23-25, 2008
F32
Hidenori Ohashi, Taichi Ito, Takeo Yamaguchi,
Development of A Novel Microscopic Free Volume Theory for Self-Diffusivity Prediction in Polymer Matrices
２３）第 57 回 高分子討論会
大阪市立大学 杉本キャンパス
2008 年 9 月 24 日 -26 日
2I10

黒木 秀記・大橋 秀伯・伊藤 大知・山口 猛央
生体分子認識ゲート膜における細孔内グラフトポリマーのナノ構造制御
２４）化学工学会 第 40 回秋季大会
東北大学
川内北キャンパス
2008 年 9 月 24 日-26 日
P316
平出 篤志・田巻 孝敬・大橋 秀伯・伊藤 大知・山口 猛央
新規ナノ構造制御酵素集積型バイオ燃料電池の開発
２５）化学工学会 第 40 回秋季大会
東北大学
川内北キャンパス
2008 年 9 月 24 日-26 日
F202
藤井 啓太朗・ 山口 猛央・伊藤 大知・大橋 秀伯
固体高分子形アルカリ燃料電池用新規芳香族系細孔フィリングアニオン交換膜の開発
２６）化学工学会 第 40 回秋季大会
東北大学
川内北キャンパス
2008 年 9 月 24 日-26 日
F201
豊田 将平・ 大橋 秀伯・伊藤 大知・山口 猛央
細孔フィリング電解質膜を用いた固体高分子形アルカリ燃料電池の開発
２７）Second International Conference on Polymer blends, Composites, IPNS, Membranes, Polyelectrolytes and Gels: Macro to Nano Scales
India
September 22-24,2008
Invited speaker
Hidenori Ohashi, Taichi Ito and Takeo Yamaguchi
Bio-Inspired Material Development according to the Notion of "Material System" and Prediction Tool of Molecular Diffusivity in Polymeric Systems for Material Design
２８）
National Institute for Interdisciplinary Science & Technology
National Institute for Interdisciplinary Science & Technology, India
September 19, 2008
Invited lecture
Hidenori Ohashi, Taichi Ito and Takeo Yamaguchi
Bio-Inspired Material Development according to the Notion of "Material System" and Prediction Tool of Molecular Diffusivity in Polymeric Systems for Material Design
２９）
化学工学会新潟大会 2008
新潟大学
2008 年 8 月 21 日-22 日
PC110
（ポスター）
黒木秀記・大橋秀伯・伊藤大知・

山口猛央
生体分子認識ゲート膜を用いたバイオセンサー開発におけるナノ細孔構造制御
３０）
International Congress on Membranes and Membrane Process 2008
Sheraton Waikiki Hotel, Honolulu, Hawaii USA
July 12-18, 2008
75(Poster)
Nobuo Hara, Taichi Ito, Takeo Yamaguchi
Development, Microstructure and Properties of Novel Wholly Aromatic Pore-Filling Electrolyte Membranes for PEFCs and DMFCs
３１）
International Congress on Membranes and Membrane Process 2008
Sheraton Waikiki Hotel, Honolulu, Hawaii USA
July 12-18, 2008
56(Poster)
Hidenori Kuroki, Taichi Ito, Takeo Yamaguchi
Development of Nobel Biomolecule-Responsive Gating System using Biomolecular Recognition Gating Membrane
３２）
International Congress on Membranes and Membrane Process 2008
Sheraton Waikiki Hotel, Honolulu, Hawaii USA
July 12-18, 2008
Hidenori Ohashi, Taichi Ito, Takeo Yamaguchi
Development of a Microscopic Free Volume Theory for Molecular Self-Diffusivity Prediction in Polymeric Systems
３３）
International Congress on Membranes and Membrane Process 2008
Sheraton Waikiki Hotel, Honolulu, Hawaii USA
July 12-18, 2008
Taichi Ito, Takeo Yamaguchi
Fixed-Charge Group-Like Behavior of the Captured Ion by Crown Ether and Its Effect on the Response of a Molecular Recognition Ion Gating Membrane
３４）日本膜学会
第 30 回年会
東京理科大学　森戸記念館
2008 年 5 月 15 日-16 日
A-1
黒木秀記・伊藤大知・山口猛央
生体分子応答ゲート膜におけるナノ細孔構造制御

H.知的財産権の出願・登録状況
１．特許取得
予定 2 件
２．実用新案登録
該当なし
３．その他
特記事項なし

別添４　　厚生労働科学研究費補助金分担研究年度終了報告書

若手研究で研究代表者が全研究を分担するために、該当なし。

別添５　研究成果の刊行に関する一覧表

書籍

著者氏名	論文タイトル名	書籍全体の編集者名	書籍名	出版社名	出版地	出版年	ページ
伊藤大知 山口猛央	多孔体へのプラズマグラフト重合を用いたバイオ材料システムの開発		多孔体の精密制御と機能・物性評価	サイエンス＆テクノロジー	東京	2008	461-468

雑誌

発表者氏名	論文タイトル名	発表誌名	巻号	ページ	出版年
Nobuo Hara, Hidenori Ohashi, Taichi Ito, Takeo Yamaguchi	Reverse response of an ion recognition polyampholyte to specific ion signals at different pHs	*Macromolecules*	42	980-986	2008
Miyaoi Naoko, Hidenori Ohashi, Taichi Ito, Takeo Yamaguchi	An Analysis of Pore Size Using a Straight-Pore Molecular Recognition Ion Gating Membrane	*Journal of Chemical Engineering of Japan*	41	766-770	2008
Hidenori Ohashi, Taichi Ito, Takeo Yamaguchi	A New Free Volume Theory Based on Microscopic Concept of Molecular Collisions for Penetrant Self-diffusivity in Polymers	*Journal of Chemical Engineering of Japan*	42	86-96	2009

Reverse Response of an Ion-Recognition Polyampholyte to Specific Ion Signals at Different pHs

Nobuo Hara,[†] Hidenori Ohashi,[‡] Taichi Ito,[‡] and Takeo Yamaguchi*[,†,‡]

Department of Chemical System Engineering, The University of Tokyo, 7-3-1 Hongo, Bunkyo-ku, Tokyo 113-8656, Japan, and Chemical Resources Laboratory, Tokyo Institute of Technology, Nagatsuta 4259, Midori-ku, Yokohama 226-8503, Japan

Received August 27, 2008; Revised Manuscript Received October 24, 2008

ABSTRACT: We synthesized and characterized for the first time an ampholytic ion-recognition linear copolymer of [3-(methacryloylamino)propyl]trimethylammonium chloride (MAPTAC), acrylic acid (AA), and benzo[18]crown-6-acrylamide (BCAm). In this copolymer, the MAPTAC unit has a positive charge. The AA unit has a negative charge that depends on the pH. The crown receptor of the BCAm unit forms a complex with specific ions such as Ba^{2+} because of the high complex formation constant which behaved like a fixed positive charge. Thus, the copolymers behaved as an ion-recognition polyampholytes and shrank at a pH equal to the isoelectric point (IEP), which shifted to a higher pH when the BCAm complexed with a cation. At that time, the BCAm also became hydrophilic with water of hydration accompanied by the cation. As a result of the combination of these two effects, we found that the reverse behaviors of swelling and shrinking occurred at different pHs in response to the same ion signal.

Introduction

Biopolymers such as protein, DNAs, and RNAs are known to have various intramolecular interactions, such as electrostatic, hydrophilic, and hydrophobic interactions, as well as hydrogen bonds. These interactions are considered to be among the important factors in determining the structures and functions of biopolymers. Biopolymers also show many functions in response to molecular signals. In the case of proteins, phosphorylation/dephosphorylation usually changes the polymer's function. In the case of DNAs, polymer function is mainly controlled by methylation.

Some synthetic molecular-signal-responsive polymers and hydrogels have also been reported, insprired by the functions of biopolymers. A lectin-loaded cross-linked polymer network of *N*-isopropylacrylamide (NIPAM) showed distinct swelling behavior in response to different saccharides.[1] A temperature-sensitive hydrogel copolymerized via molecular imprinting showed a volume change in response to specific molecules.[2] An antigen–antibody semi-IPN hydrogel showed reverse swelling behavior in a buffer solution in response to a specific antigen.[3] These previous researches utilized the change in cross-linking density or hydration condition induced by molecular signals but did not utilize the electrostatic interaction.

Recently, there has been much interest in polyampholytes because they have many similarities to biopolymers such as proteins.[4] The polymer chain of polyampholytes contains both cationic and anionic groups, and the balance of positively and negatively charged groups can be controlled by changing the monomer content in the feed solution.[5,6] The balance of positively and negatively charged groups also changes when these charged groups are sensitive to the pH of the solution. Synthetic polyampholytes have an isoelectric point (IEP) at a specific pH, where the polymer chain is electroneutral and shrinks.[7] The synthetic polyampholytes also show the antipolyelectrolyte effect, in which the polymer chain is soluble at the IEP because of the electric shielding of the fixed charges due to a high salt concentration.[8] However, this electrostatic interaction has not been controlled by molecular signals.

Many synthetic host compounds such as crown ethers[9] and cryptand complexes[10,11] have been designed and analyzed in the field of supramolecular chemistry.[10] Benzo[18]crown-6-acrylamide (BCAm), one of the molecular recognition compounds, has a crown ether receptor and traps specific ions such as K^+ and Ba^{2+}.[12] The copolymer of NIPAM and BCAm was synthesized, and the shift in the lower-critical-solution temperature was observed when the BCAm captured specific ions.[13] Recently, we hypothesized on the basis of our previous researches that captured ions behaved like fixed positive charges when the BCAm formed a complex with a specific ion because of the osmotic pressure generated by the Donnan exclusion-like effect under a specific ion concentration gradient.[14] In addition, we found that the complex of a BCAm and a specific ion retains about 70–80 water molecules and makes the polymer chain more hydrophilic.[15]

In this research, we synthesized a linear copolymer of MAPTAC, AA, and BCAm (Figure 1). Its phase-separation behavior in response to pH, ion species, and salt concentration was investigated. The effect of the composition of the copolymers was also studied. MAPTAC has a stable quaternary ammonium base, amide bond, and propyl group, while AA has a pH-sensitive carboxylic acid group.[16] The molecular structure of poly-MAPTAC-*co*-AA-*co*-BCAm contains both positively and negatively charged groups and well-balanced molecular interactions, such as electrostatic, hydrophilic, and hydrophobic interactions, as well as hydrogen bonds. In addition, complex formation between BCAm and ions has the above-mentioned unique physicochemical effects, which are expected to trigger unique phase-separation phenomena of the copolymer.

Experimental Section

Materials. [3-(Methacryloylamino)propyl]trimethylammonium chloride (MAPTAC, 50 wt % aqueous solution) was purchased from Aldrich Co., Ltd.; inhibitor was removed using an adsorption column before polymerization. Acrylic acid was purchased from Wako Chemical Co., Ltd., and purified by distillation. BCAm was synthesized according to reported procedures.[12] 2,2′-Azobis(2-methylpropionamidine) dihydrochloride (V-50) was purchased from Wako Chemical Co., Ltd., and used as an initiator. Standard aqueous

* Corresponding author: Tel +81-45-924-5254; Fax +81-45-924-5253; e-mail yamag@res.titech.ac.jp.
† The University of Tokyo.
‡ Tokyo Institute of Technology.

10.1021/ma801936t CCC: $40.75
Published on Web 01/30/2009

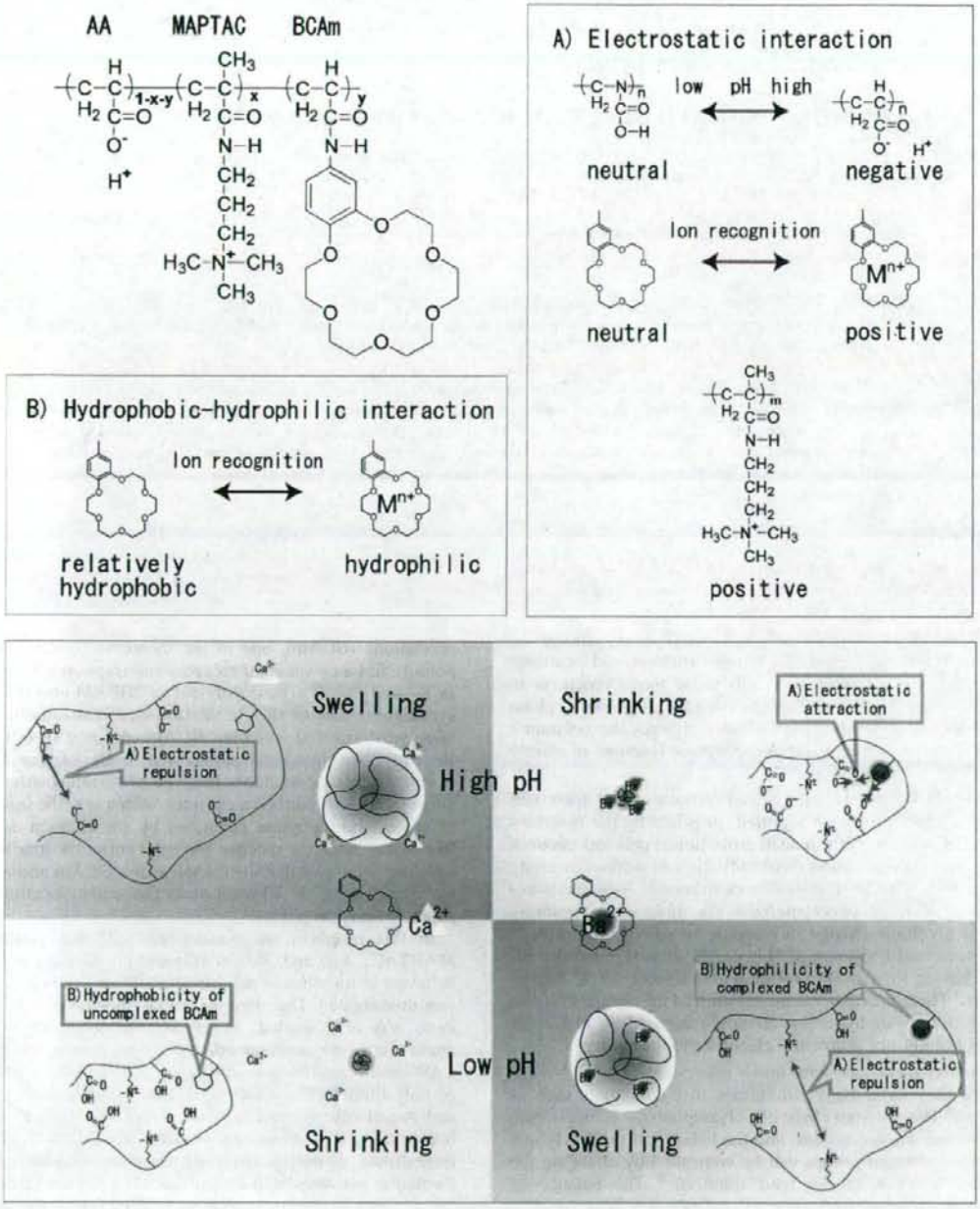

Figure 1. Chemical structure, intramolecular interactions, and concept of molecular-recognition response of poly-MAPTAC-*co*-AA-*co*-BCAm.

solutions of hydrochloric acid and sodium hydroxide were purchased from Wako Chemical Co., Ltd., and used for IEP measurements and turbidimetric titrations.

Preparation of the Linear Copolymer. Poly-MAPTAC-*co*-AA-*co*-BCAm was synthesized by free-radical copolymerization. The molar copolymerization ratios were controlled according to Table 1. Aqueous solutions of MAPTAC, AA, and BCAm were prepared from degassed RO water. The ratio of initiator was fixed at 0.5 mol % for all monomers, and the weight percentage of monomers was fixed at 15 wt %. The aqueous solution was kept at 50 °C for 48 h under N_2 after initiating polymerization by visible light for 12 min. The copolymer was dissolved in RO water, purified by dialysis—using a dialysis membrane for which the molecular weight cutoff was about 12 000—and dried under vacuum. Chloride ions contained in the aqueous monomer solution of MAPTAC were also removed by dialysis after polymerization.

Characterization. The synthesized linear copolymers were characterized by FT-IR, elemental analysis, and UV−vis spectroscopy. The FT-IR spectrum of the linear copolymer was measured using the KBr disk technique with an MGNA 550 (Nicolet). Elemental analysis was performed on a 2400II (Perkin-Elmer). The UV−vis spectrum of the linear copolymer was measured using a U-3310 (Hitachi). The absorption intensities in the UV−vis spectrum were measured using an aqueous solution of copolymers.

Table 1. Molar Compositions of the Monomer Solutions and Copolymers, with MAPTAC, AA, and BCAm Content as 100 mol %[a]

composition of monomer solutions				copolymerization ratio		
[mol %]	MAPTAC	AA	BCAm	MAPTAC	AA	BCAm
(a)	100			100		
(b)	38	62		39	61	
(c)	24	76		25	75	
(d)	18	82		18	82	
(e)	14	43	43	12	39	49
	(24)	(76)	(76)	(23)	(77)	(96)
(f)	12	57	30	9	65	26
	(18)	(82)	(42)	(12)	(88)	(35)

[a] Compositions with MAPTAC and AA content as 100 mol % are shown in parentheses.

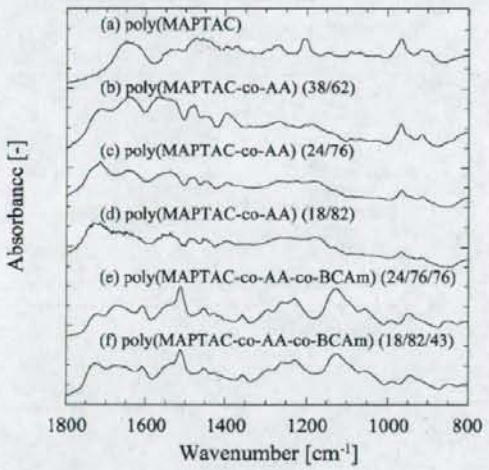

Figure 2. FT-IR spectra of poly(MAPTAC), poly(MAPTAC-*co*-AA), and poly(MAPTAC-*co*-AA-*co*-BCAm).

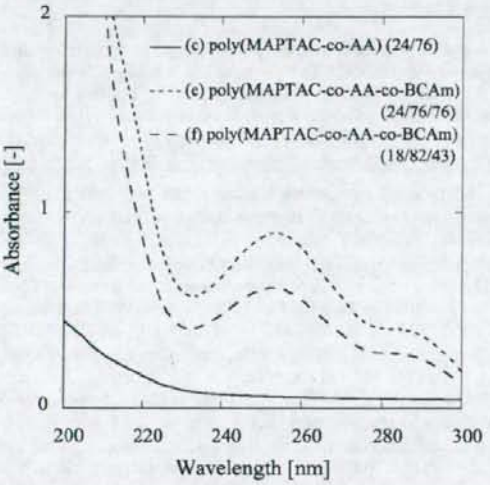

Figure 3. UV spectra of poly(MAPTAC-*co*-AA) and poly(MAPTAC-*co*-AA-*co*-BCAm).

Turbidimetric Measurement. Copolymer solutions change turbidity when copolymer chains shrink, and this behavior was measured spectrophotometrically as the optical density at 650 nm. Turbidimetric titration of the linear copolymer solution was performed in 0.2 wt % copolymer concentration at 25 °C. The pH was first changed to about pH 2 by adding 0.01 M HCl aqueous solution, and it was then changed to pH 12 by adding 0.01 M NaOH aqueous solution in 10 μL aliquots. Each time, the pH was measured using a pH meter HM21P (TOD-DKK), and the optical density was measured. Measurements were carried out a few minutes after titration to obtain a stable optical density value. The turbidimetric titration of the linear copolymer solution was also carried out with various concentrations of $CaCl_2$, $SrCl_2$, and $BaCl_2$. Turbidity changes were also measured by adding 0.1 M aqueous solution of $CaCl_2$, $SrCl_2$, and $BaCl_2$ in 10 μL aliquots in both acid and base conditions and by alternately adding 0.1 M aqueous solution of $BaCl_2$ and [18]crown-6.

Results and Discussion

Characterization of Copolymers. Figure 2 shows the FT-IR spectra of the copolymers. Copolymerization of MAPTAC, AA, and BCAm was determined by FT-IR measurements. The peaks are 1650 cm^{-1} from the amide bond of MAPTAC, 1720 cm^{-1} from the carboxyl group of AA, and 1133 cm^{-1} from the ether group of BCAm. Figure 3 shows the UV spectra of copolymers of BCAm, which had an absorbance peak at 255 nm. The copolymerization ratio of BCAm was estimated from the following proportional relationship between the absorbance at 255 nm and concentration of poly-BCAm:

$$C_{BCAm} = 1.21 \times 10^{-4} a \text{ mol/L} \quad (1)$$

where a is the absorbance at 255 nm and C_{BCAm} is the concentration of poly-BCAm.[17] The copolymerization ratio of MAPTAC to AA was determined by the weight ratio of carbon and nitrogen atoms obtained from elemental analysis. The total molar copolymerization ratios MAPTAC:AA:BCAm determined from these measurements are shown in Table 1. These molar copolymerization ratios are in close agreement with those used in the synthesis. The molar copolymerization ratios are shown for MAPTAC, AA, and BCAm content as 100 mol %.

pH Dependence of Poly(MAPTAC), Poly(MAPTAC-*co*-AA), and Poly(MAPTAC-*co*-AA-*co*-BCAm). In general, a polyampholyte shrinks at a pH equal to the IEP, where the positive and negative charges balance and the solution of linear copolymer becomes turbid.[5,18] The monomer of MAPTAC is a chloride ion salt, and poly(MAPTAC) acts as a positive charge whose amount is not affected by pH (Figure 1). AA is a weak acid, and it acts as a negative charge whose magnitude is affected by the degree of dissociation. Thus, the balance of positive and negative charges changes depending on the pH of the solution. The amount of negative charge is low because of the low degree of dissociation of AA at pHs below the IEP, while negative and positive charges balance when the pH equals the IEP, and negative charges exceed positive charges at pHs above the IEP. Since the dissotiation degree α of weak acid relates to pH by the following equation

$$\mathrm{pH} = \mathrm{p}K_a + \log\left(\frac{\alpha}{1-\alpha}\right) \quad (2)$$

the pH of the IEP where the ratio of the positive and the negative charges inside the linear polymer balance can be estimated. Using $pK_a = 4.25$ previously reported for poly(acrylic acid),[19] the pH of the IEP was calculated as 4.5, 3.9, 3.7, 3.9, and 3.7 for copolymer (b), (c), (d), (e), and (f) respectively, for (e) and (f) without considering the effect of the copolymerized BCAm.

Figure 4 shows the pH dependencies for the turbidimetric titrations of the 0.2 wt % aqueous copolymer solutions of poly(MAPTAC), poly(MAPTAC-*co*-AA), and poly(MAPTAC-*co*-AA-*co*-BCAm). The absorbance of the aqueous polymer solution of (a) poly(MAPTAC) is low over the entire pH range. This is because poly(MAPTAC) contains only positive charges

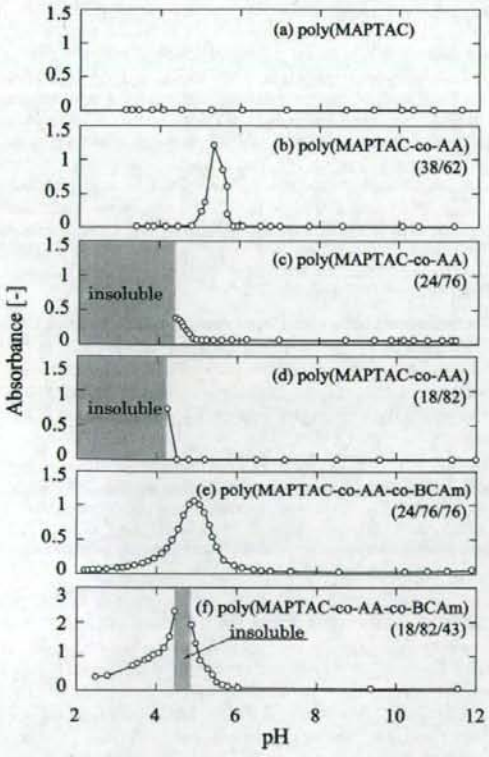

Figure 4. pH dependence of poly(MAPTAC-*co*-AA) and poly(MAPTAC-*co*-AA-*co*-BCAm).

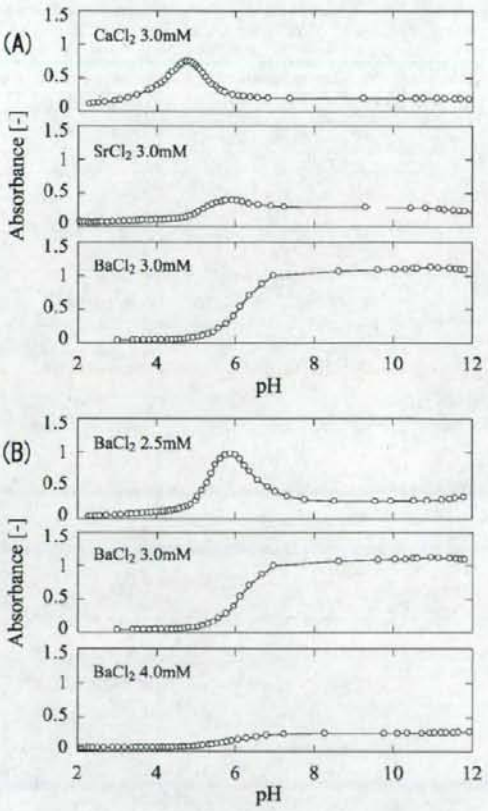

Figure 5. pH dependence of the copolymer used in Figure 4e, poly(MAPTAC-*co*-AA-*co*-BCAm) (24/76/76), with salt. (A) Different ion species of $CaCl_2$, $SrCl_2$, and $BaCl_2$. (B) Concentration dependence of $BaCl_2$.

inside the polymer chain and is always swollen by electrostatic repulsion. The absorbance of copolymers of poly(MAPTAC-*co*-AA) varied according to the pH of the solution. A 0.2 wt % aqueous solution of copolymer (b) turned turbid at about pH 5.4; copolymers (c) and (d) turned turbid and resulted in precipitation below pH 4.4 and 4.2, respectively. Copolymers (e) and (f) have the same ratio of MAPTAC to AA as copolymers (c) and (d) and contain BCAm with 43 and 30 mol %, respectively. The 0.2 wt % aqueous solution of copolymer (e) turned turbid at about pH 5.0; copolymer (f) turned turbid and resulted in precipitation at about pH 4.6. However, these values of pH were higher than the pH of the IEP estimated by the calculation; their trends were almost the same according to the monomer compositions. Therefore, behavior as a polyampholyte was confirmed for the aqueous solution of both poly(MAPTAC-*co*-AA) and poly(MAPTAC-*co*-AA-*co*-BCAm). Their differences are expected to be due to the different value of pK_a from the reported value with different component of the copolymerization.

Thus, a solution of copolymer (b) turned turbid when the pH equaled the IEP. Solutions of copolymers (c) and (d) turned turbid and resulted in precipitation because the copolymer of high AA content could reach the IEP with low degree of dissociation and also because of the hydrogen bond between dissociated AA[20] and the relatively hydrophobic uncomplexed BCAm. The pH of the IEP of copolymers (e) and (f) were measured to be about 0.5 higher than those of copolymers (c) and (d). Copolymers (e) and (f) were more soluble than (c) and (d), probably because the difference of the value of pK_a and the ratio of hydrogen bonds was decreased by copolymerization with BCAm.

The concentration of the Na^+ ion after turbidimetric titration was about 10 mM. The peak of the turbidity of the IEP was observed at the same pH reproducibly by multicycle measurement of the titration; however, the peak height slightly decreased because of the increase of the concentration of the added salt, which is called the anti-polyelectrolyte effect.

Different Ion Species Changed the IEP Shift. The result for copolymer (e) will be explained after the next two sections. Figure 5A shows the pH dependence for the turbidimetric titrations of 0.2 wt % aqueous polymer solution of poly(MAPTAC-*co*-AA-*co*-BCAm) in the presence of various salts. The concentration of the salts $CaCl_2$, $SrCl_2$, and $BaCl_2$ was controlled to 3.0 mM at the beginning of the titration. BCAm forms complexes with various ions, and the complex formation constants increase in the order Ca^{2+}, Sr^{2+}, Ba^{2+}.[21] The balance of charges inside the polymer chain is also estimated from the complex formation constant K and eq 2 by considering the complexed divalent ions into positive charges. Using $\log K =$ 1.1 and 1.6 for Sr^{2+} and Ba^{2+}, respectively, which were previously reported for poly-NIPAM-*co*-BCAm,[17] the pH of the IEP shifted higher by 0.1 and 0.5 in the presence of 3.0 mM ions.

An aqueous solution of copolymer in the presence of 3.0 mM Ca^{2+} ions turned turbid at about pH 4.9. The pH at the IEP did not shift from that of the same titration without Ca^{2+} ions because the complex formation constant of BCAm and Ca^{2+} ion is low, and the positive charges were not introduced inside

the polymer chain. The copolymer also became soluble, and the absorbance decreased because of the anti-polyelectrolyte effect in the presence of $CaCl_2$ salt. An aqueous solution of the copolymer in the presence of 3.0 mM Sr^{2+} ions turned turbid at about pH 5.9. The pH at the IEP shifted by about 1.0 compared with that of the same titration without Sr^{2+} ions. This was because BCAm and Sr^{2+} ions formed complexes and positive charges were introduced inside the copolymer chain. The solution of the copolymer also became soluble, and the absorbance decreased because of the hydrophilic change of complexed BCAm and the antipolyelectrolyte effect. An aqueous solution of copolymer in the presence of 3.0 mM Ba^{2+} ion turned turbid at a pH of about 6.0. This is because the complex formation constant of BCAm and Ba^{2+} ion is high. The total positive charges of MAPTAC and those introduced inside the copolymer chains are in balance with the negative charges of dissociated AA, and the polymer chain remained at the IEP in the higher pH range. Although the observed shift range of the pH is wider than the calculated values, their trends are well consistent with the order of the complex formation constant. Their differences are expected to be due to the difference of the values of complex formation constant, which are widely different according to the copolymerization systems and other effects such as hydrophilic change of complexed BCAm.

Figure 5B shows the pH dependence for the turbidimetric titrations of 0.2 wt % of aqueous polymer solution of poly(MAPTAC-*co*-AA-*co*-BCAm) in the presence of various concentrations of $BaCl_2$, namely 2.5, 3.0, and 4.0 mM. An aqueous solution of the copolymer in the presence of 2.5 mM Ba^{2+} ion turned turbid at about pH 5.9 by complexation of BCAm and Ba^{2+} ions. An aqueous solution of the copolymer in the presence of 4.0 mM Ba^{2+} ions became slightly turbid above a pH of about 6.0. The number of total positive charges on MAPTAC and those introduced inside the copolymer chains exceeds the number of negative charges on the dissociated AA. The polymer chain did not reach the IEP, and the solution turned slightly turbid. The anti-polyelectrolyte effect with high salt concentration and hydrophilic change of complexed BCAm were also reasons for the low absorbance.

From these results, positive charges were introduced into the polymer chain by complex formation of BCAm and cations depending on the complex formation constant and the concentration of the cation. The behaviors of swelling and shrinking of polymer chains and the amount of positive charge inside the polymer chains were controlled by the species and the concentration of the ion.

Ion Recognition Changed by an Anti-polyelectroyte Effect. Figure 6A shows the turbidimetric measurements of 0.2 wt % aqueous copolymer solutions upon gradually adding 0.1 M solutions of various salts at pH 5.0, where the copolymer was at the IEP without salt. The polymer initially shrank at the IEP and gradually changed to swelling by the addition of salt solution. The absorbance decreased in the order of Ba^{2+}, Sr^{2+}, Ca^{2+}, which is the order of the complex formation constants. This is because of the IEP shift to higher pH by complex formation of BCAm and the cation, and there is also the influence of the anti-polyelectrolyte effect.

Figure 6B shows the turbidimetric measurements of 0.2 wt % copolymer solution upon gradually adding 0.1 M solution of various salts at pH 11.6. The copolymer was initially swollen and gradually changed to shrinking by the addition of salt solution. The absorbance increased in the order Ba^{2+}, Sr^{2+}, Ca^{2+}, which is the order of the complex formation constants. The carboxylic groups of AA are all dissociated at pH 11.6, and negative charges are initially in excess. Positive charges are introduced into the copolymer chain by complex formation between BCAm and the cation. The polymer chain started to

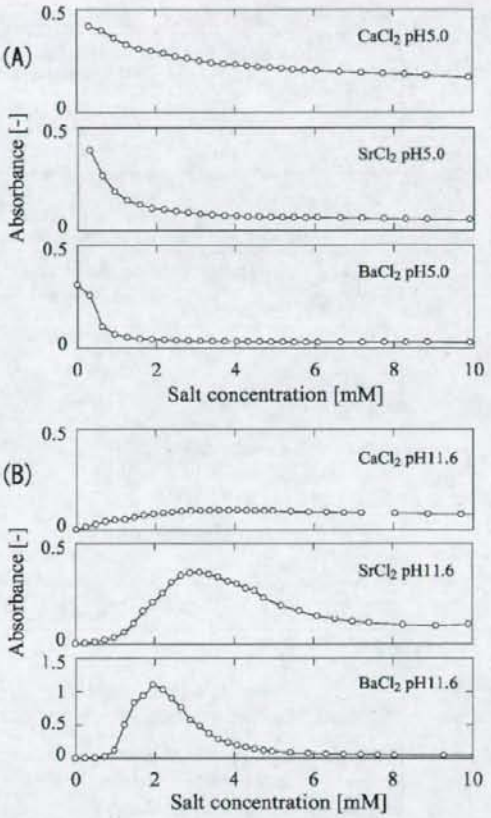

Figure 6. Salt concentration dependence of the copolymer (e) (poly-MAPTAC-*co*-AA-*co*-BCAm) (24/76/76). (A) Different ion species of $CaCl_2$, $SrCl_2$, and $BaCl_2$. (B) Concentration dependence of $CaCl_2$, $SrCl_2$, and $BaCl_2$.

shrink at the point where the positive charges balanced the negative charges. When the number of positive charges exceeded the number of negative charges, the polymer chain started swelling again. We also deduce from these results that the number of positive charges inside the polymer chain was controlled by the species and the concentration of ions, and the antipolyelectrolyte effect crucially affected the behavior.

There is another expected effect of adding divalent ions, which dissociated carboxylic groups can be cross-linked by divalent ions above the pH of the IEP. It is understood mainly by electrostatic interaction on their charge size ratio measured in terms of ionic radii.[22] Thus, the interaction of added divalent ions decreases in the order of Ca^{2+}, Sr^{2+}, and Ba^{2+}. This interaction is expected to exist in the copolymer chain when divalent ion is added into the solution. However, from the Figure 6B, the copolymer chain shrank more in the order of high complex forming constant with BCAm, not in the order of the strength of the cross-link of the divalent ion. From this result, the effect of complex forming of BCAm with Ba^{2+} is thought to be stronger than the effect of the cross-link of the divalent ion. Therefore, we speculate that the effect of the cross-link by divalent ions is not obvious because the electrostatic interaction between the dissociated AA and the complexed BCAm is thought to be dominant in this copolymer system.

Reverse Response of Poly(MAPTAC-*co*-AA-*co*-BCAm) to Specific Ions at Different pHs. Parts A and B of Figure 7 show the alternate salt addition of $BaCl_2$ and [18]crown-6 to

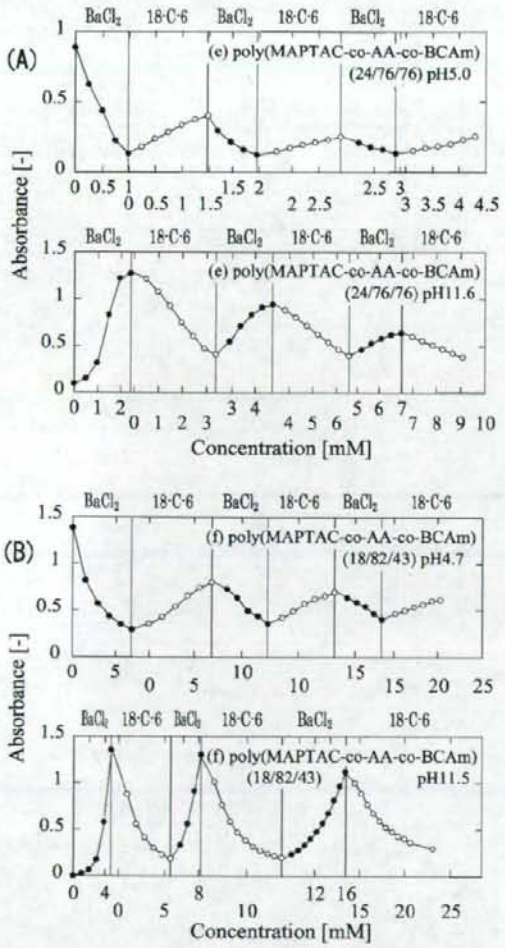

Figure 7. Turbidity change of the aqueous solutions of copolymers (e) and (f) by alternately adding $BaCl_2$ and [18]crown-6 aqueous solutions.

0.2 wt % aqueous copolymer solutions of (e) and (f), respectively. Turbidity was measured both at the IEPs and higher pHs of alkaline conditions. [18]Crown-6 can remove Ba^{2+} ions from the polymer chain because the complex formation constant of [18]crown-6 is higher than that of BCAm. Therefore, Ba^{2+} ions can be alternately introduced into the polymer chain by adding a 0.1 M aqueous solution of Ba^{2+} and [18]crown-6.

In this measurement, the behavior of swelling and shrinking was observed for both copolymers (e) and (f). The copolymer initially shrank when the pH was at the IEP and then changed to swelling by adding Ba^{2+} ions. The copolymer began shrinking again by adding [18]crown-6, and this behavior was observed alternately. The copolymer initially swelled in alkaline conditions then changed to shrinking by adding Ba^{2+} ions. The copolymer changed to swelling again by adding [18]crown-6, and this behavior was also observed alternately. The absorbance of the copolymer solution in the shrinking condition gradually decreased because of the anti-polyelectrolyte effect caused by the increase in the concentration of salt and [18]crown-6. The response of the absorbance change to salt concentration of copolymer (e) was more sensitive than for copolymer (f). This is because copolymer (e) has a higher molar composition of BCAm than copolymer (f).

Thus, we demonstrated the alternate swelling and shrinking behavior of an aqueous solution of poly(MAPTAC-*co*-AA-*co*-BCAm) by alternately adding a 0.1 M aqueous solution of Ba^{2+} and [18]crown-6. The behaviors of swelling and shrinking in response to the same ion addition were completely opposite under acidic and alkaline conditions.

Conclusions

We synthesized and characterized for the first time an ion-recognition polyampholyte. The copolymers of poly(MAPTAC-*co*-AA-*co*-BCAm) showed the behavior of polyampholytes and shrank when the pH equaled the IEP, which was shifted by the ion signal recognized by BCAm, which can form a complex with specific ions depending on the complex formation constant and the concentration of the ions. The intramolecular interactions, mainly electrostatic interactions, were controlled by ion recognition of BCAm and the pH of the solution, which led to the swelling and shrinking behaviors of the copolymer in response to both pH and ion recognition. We found that the reverse behaviors of swelling and shrinking occurred at a different pHs in response to the same ion signal. These phenomena are complicated and interesting, especially in terms of similarity to biopolymers, which respond to the same signal in different ways depending on changes in the external environment such as pH and temperature. The concept of macromolecular design in the present research is expected to be utilized in fields such as separation technology, biomaterials, and drug-delivery systems in the future.

References and Notes

(1) Kokufata, E.; Zhang, Y. Q.; Tanaka, T. *Nature (London)* **1991**, *351* (6324), 302–304.
(2) (a) Wulff, G. *Angew. Chem., Int. Ed.* **1995**, *34* (17), 1812–1832. (b) Watanabe, M.; Akahoshi, T.; Tabata, Y.; Nakayama, D. *J. Am. Chem. Soc.* **1998**, *120* (22), 5577–5578.
(3) (a) Miyata, T.; Asami, N.; Uragami, T. *Macromolecules* **1999**, *32* (6), 2082–2084. (b) Miyata, T.; Asami, N.; Uragami, T. *Nature (London)* **1999**, *399* (6738), 766–769.
(4) Kudaibergenov, S. E. *Polyampholytes: Synthesis, Characterization, and Application*; Kluwer Academic/Plenum Press: New York, 2002; p 220.
(5) Kudaibergenov, S. E.; Sigitov, V. B. *Langmuir* **1999**, *15* (12), 4230–4235.
(6) Mccormick, C. L.; Salazar, L. C. *Macromolecules* **1992**, *25* (7), 1896–1900.
(7) (a) Baker, J. P.; Stephens, D. R.; Blanch, H. W.; Prausnitz, J. M. *Macromolecules* **1992**, *25* (7), 1955–1958. (b) Skouri, M.; Munch, J. P.; Candau, S. J.; Neyret, S.; Candau, F. *Macromolecules* **1994**, *27* (1), 69–76.
(8) (a) Corpart, J. M.; Candau, F. *Macromolecules* **1993**, *26* (6), 1333–1343. (b) Patrickios, C. S.; Sharma, L. R.; Armes, S. P.; Billingham, N. C. *Langmuir* **1999**, *15* (5), 1613–1620.
(9) (a) Higgins, S. J. *Chem. Soc. Rev.* **1997**, *26* (4), 247–257. (b) Cacciapaglia, R.; Mandolini, L. *Chem. Soc. Rev.* **1993**, *22* (4), 221–231. (c) Olsher, U.; Izatt, R. M.; Bradshaw, J. S.; Dalley, N. K. *Chem. Rev.* **1991**, *91* (2), 137–164.
(10) Schneider, H. J.; Yatsimirsky, A. K. *Chem. Soc. Rev.* **2008**, *37* (2), 263–277.
(11) Lincoln, S. F. *Coord. Chem. Rev.* **1997**, *166*, 255–289.
(12) (a) Ungaro, R.; Haj, B. E.; Smid, J. *J. Am. Chem. Soc.* **1976**, *98* (17), 5198–5202. (b) Yagi, K.; Ruiz, J. A.; Sanchez, M. C. *Makromol. Chem., Rapid Commun.* **1980**, *1* (4), 263–268.
(13) (a) Irie, M. *Adv. Polym. Sci.* **1993**, *110*, 49–65. (b) Irie, M.; Misumi, Y.; Tanaka, T. *Polymer* **1993**, *34* (21), 4531–4535.
(14) Ito, T.; Yamaguchi, T. *J. Am. Chem. Soc.* **2004**, *126* (20), 6202–6203.
(15) Ito, T.; Nishikawa, M.; Yamaguchi, T. Manuscript in preparation.
(16) (a) Annaka, M.; Tanaka, T. *Nature (London)* **1992**, *355* (6359), 430–432. (b) Shibayama, M.; Tanaka, T. *Adv. Polym. Sci.* **1993**, *109*, 1–62. (c) Hirokawa, Y.; Tanaka, T.; Sato, E. *Macromolecules* **1985**, *18* (12), 2782–2784.

(17) Ito, T.; Sato, Y.; Yamaguchi, T.; Nakao, S. *Macromolecules* **2004**, *37* (9), 3407–3414.
(18) Kudaibergenov, S. E.; Didukh, A. G.; Zhumadilova, G. T.; Koizhaiganova, R. B.; Bimendina, L. A.; Noh, J. G.; Geckeler, K. E. *Macromol. Symp.* **2004**, *207*, 153–171.
(19) Ende, M. T. A.; Peppas, N. A. *J. Appl. Polym. Sci.* **1996**, *59* (4), 673–685.
(20) Karino, T.; Masui, N.; Hiramatsu, M.; Yamaguchi, J.; Kurita, K.; Naito, S. *Polymer* **2002**, *43* (26), 7467–7475.
(21) Izatt, R. M.; Bradshaw, J. S.; Nielsen, S. A.; Lamb, J. D.; Christensen, J. J. *Chem. Rev.* **1985**, *85* (4), 271–339.
(22) Rotello, V. E. *Nanoparticles Building Blocks for Nanotechnology*; Kluwer Academic/Plenum Publishers: New York, 2004; pp 225–250.

MA801936T

Analysis of Pore Size Using a Straight-Pore Molecular Recognition Ion Gating Membrane

Naoko MIYAOI[1], Hidenori OHASHI[1],
Taichi ITO[2] and Takeo YAMAGUCHI[1,2]
[1]*Department of Chemical System Engineering, The University of Tokyo, 7-3-1, Hongo, Bunkyo-ku, Tokyo 113-8656, Japan*
[2]*Chemical Resources Laboratory, Tokyo Institute of Technology, R1-17, 4259, Nagatsuta-cho, Midori-ku, Yokohama-shi, Kanagawa 226-8503, Japan*

Keywords: Molecular Recognition, Ion Gating Membrane, Cylindrical Pore, Water Permeability, Hagen–Poiseuille Equation

An analysis of the water permeability of a molecular recognition ion gating membrane was performed. The ion gating membrane shows outstanding water permeability switching properties in response to specific ion concentrations, using an ion-responsive polymer consisting of thermosensitive poly(*N*-isopropylacrylamide) and crown ether moieties, grafted onto a porous substrate pore surface. To investigate the precise properties of the membrane, a polycarbonate track-etched membrane having straight pores with a narrow pore size distribution was used as the substrate, and the ion responsive polymer was grafted onto its pore surfaces. The gating property of the prepared membrane was examined as a function of temperature, specific ion concentration, and filling ratio. Estimates of pore size and dimension of the grafted polymer were obtained using the Hagen–Poiseuille equation. We found that the grafted ion-responsive polymer shows drastic dimensional changes in response to temperature and specific ion concentrations.

Introduction

The living body is a sophisticated system that expresses a range of diverse and outstanding functions. Methodologies to develop analogous functional systems using pure artificial materials are inspired by this biosystem, and this strategy is promising. Molecular recognition functionality is one of the key elements required to design distinct systems in living bodies and also in artificial devices.

Following this strategy, we have proposed a molecular recognition ion gating membrane (Yamaguchi *et al.*, 1999; Ito *et al.*, 2002). This sophisticated membrane consists of a porous membrane as a stable substrate and a grafted polymer as the ion-responsive moiety (**Figure 1**). The grafted polymer is a copolymer of *N*-isopropylacrylamide (NIPAM), which has thermoresponsive properties, and benzo-18-crown-6 acrylamide (BCAm), which recognizes specific ions (such as K^+ and Ba^{2+}) (Irie *et al.*, 1993). The ion gating membrane can close its pores in the presence of the specific ion, and can open them in the absence of that ion. The membrane shows marked ability to control water permeability in response to specific ion concentrations. However, the substrate used in the previous investigations was porous polyethylene (PE), which has complex pores and a wide pore size distribution (Yamaguchi *et al.*, 1999; Ito *et al.*, 2002), and precise information is required for analysis and application of the ion gating membrane.

Therefore, we prepared an ion gating membrane for this study using a polycarbonate track-etched membrane with straight pores and a narrow pore size distribution (Rui *et al.*, 2005; Friebe and Ulbricht, 2007) as the porous substrate, and performed an analysis of the membrane's water permeability and pore size as a function of temperature, ionic concentration, and filling ratio.

1. Experimental

1.1 Materials

Cyclopore® polycarbonate, track-etched with a porosity of 17% was used as the porous substrate, and purchased from SPI Supplies Division of Structure Probe, Inc. BCAm was synthesized from benzo-18-crown-6 using published techniques (Ungaro *et al.*, 1976; Yagi *et al.*, 1980). Benzo-18-crown-6 was purchased from Sigma-Aldrich Japan K.K., and barium chloride ($BaCl_2$) and *N*-dodecylbenzenesulfonic acid

Received on January 15, 2008; accepted on February 25, 2008.
Correspondence concerning this article should be addressed to H. Ohashi (E-mail address: hidenori@chemsys.t.u-tokyo.ac.jp).

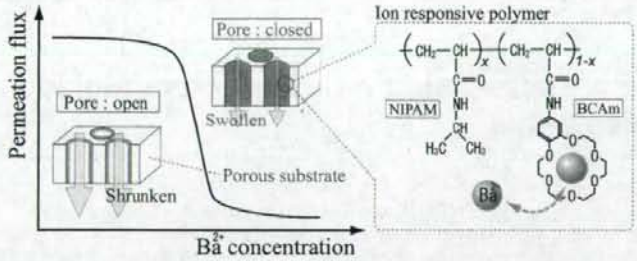

Fig. 1 Schematic representation of a molecular recognition ion gating membrane

sodium salt (SDBS) were purchased from Wako Pure Chemical Industries, Ltd. NIPAM was supplied by Kohjin Co., Ltd.

1.2 Preparation of an ion gating membrane having cylindrical pores and uniform pore size distribution

An ion gating membrane having cylindrical straight pores and uniform pore size distribution was prepared using the track-etched membrane and the plasma graft polymerization technique developed in our previous work (Yamaguchi *et al.*, 1991, 1996). The Cyclopore® was treated with argon plasma at a pressure of 10 Pa, and was then exposed to air for 60 s to generate peroxide groups on its pore surface. The substrate containing peroxide groups was immersed in an extensively degassed (frozen and thawed) aqueous solution of 5 wt% monomers of NIPAM and BCAm (the molar ratio of NIPAM to BCAm was fixed at 95:5), and 4 wt% SDBS as a surfactant. By holding the solution at 80°C, the peroxide groups were broken to form active radical sites, and a graft polymerization reaction started from the initiator radicals. The reaction time was varied from 10 to 60 min to control the filling ratio. After the grafting, any remaining monomers and surfactant were removed by rinsing the membrane with water, a 50% aqueous ethanol solution, and hexane for 1 h, respectively. Graft polymerization was evaluated by weight change, FT–IR spectra, and scanning electron microscopy (SEM). The filling ratio ϕ of the grafted membrane is defined by Eq. (1).

$$\phi\,[\%] = \frac{W_{dry} - W_{sub}}{\rho_{polym} \cdot V_{pore}} \times 100 \qquad (1)$$

where, W_{dry} [g] and W_{sub} [g] represent the weight of the grafted membrane and the nongrafted membrane substrate, respectively. ρ_{polym} [g/cm^3] is the density of the ion-responsive polymer, and is assumed to be 1.0 g/cm^3 for a copolymer of NIPAM and BCAm. V_{pore} [cm^3] is the pore volume of the substrate.

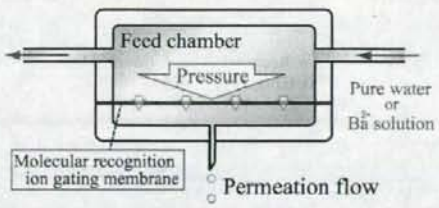

Fig. 2 Filtration apparatus to measure the permeation flux through a molecular recognition ion gating membrane

1.3 Measurement of permeation flux through the prepared molecular recognition ion gating membrane

The water permeation flux through the prepared ion gating membrane was measured. A schematic diagram of the filtration apparatus to measure the permeation flow is shown in **Figure 2**. Pure water or an aqueous $BaCl_2$ solution was passed through a feed chamber and an appropriate pressure (0.18–0.22 kg f/cm^2) was applied across the membrane. The permeation flux was calculated from the amount of permeated solution. Here, to eliminate the effect of the applied pressure and media viscosity on permeation flux J [m^3/(s cm^{-2})], the permeability coefficient L_p [m/(kg f s cm^{-2})] was used to evaluate membrane permeability. L_p is defined in Eq. (2).

$$L_p = \frac{J}{\Delta P \cdot \left(\mu_{25^\circ C}/\mu_T\right)} \qquad (2)$$

where, ΔP [kg f/m^2] is the pressure applied across the membrane, and $\mu_{25^\circ C}$ [Pa s] and μ_T [Pa s] represent media viscosity at 25°C and the measurement temperature, respectively. In this series of measurements, the $BaCl_2$ concentration was varied from 1 to 100 mM, the measurement temperature was varied from 20 to 50°C, and the filling ratio was varied from 0 to 37%.

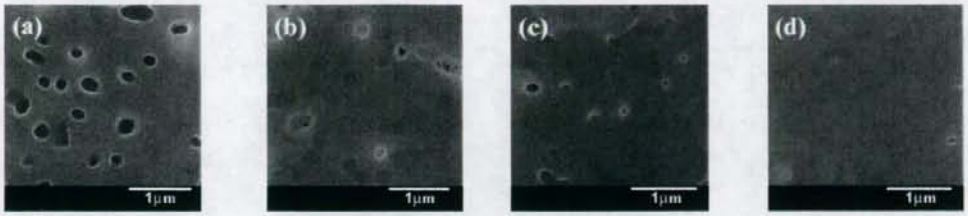

Fig. 3 Scanning electron microscopy images of poly (NIPAM-co-BCAm) grafted polycarbonate track-etched membrane; filling ratio (a) 0% (nongrafted), (b) 13.9%, (c) 31.0%, and (d) 73.4%

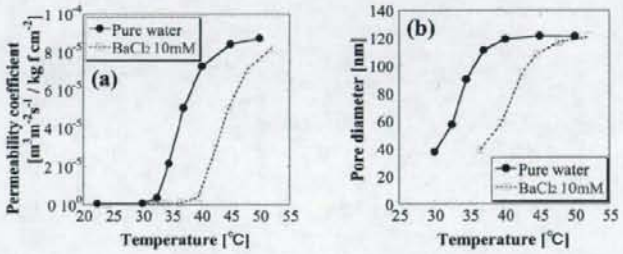

Fig. 4 Temperature dependence of permeation properties on an ion gating membrane having cylindrical straight pores (filling ratio 15.3%) for pure water and 10 mM aqueous $BaCl_2$ solution: (a) permeability coefficient; (b) pore diameter

2. Results and Discussion

2.1 Preparation of an ion gating membrane having cylindrical pores and uniform pore size distribution

From the weight difference measured before and after the graft polymerization, FT–IR spectra, and SEM images, successful polymer grafting on the PCTE substrate was confirmed. SEM images of the grafted membranes with several filling ratios are shown in the dry state in **Figure 3**. It can be seen that the pore size of the membrane becomes smaller as the filling ratio increases. With a filling ratio of 73%, the pores were almost completely filled with grafting polymer, even in their dry state. The figure also shows successful grafting on the membrane pore surface.

2.2 Measurement of permeation flux through the prepared molecular recognition ion gating membrane

The temperature dependence of the permeability coefficient for pure water and a 10 mM aqueous $BaCl_2$ solution is shown in **Figure 4(a)**. A membrane with a 15.3% filling ratio was used. Both lines show clear lower critical solution temperature (LCSTs), where the permeability drastically changes. In the presence of Ba^{2+} ions, the LCST shifts to a higher temperature. The observed LCSTs are almost the same as the LCSTs of the membrane prepared using a PE substrate (Ito *et al.*, 2002). To examine the effect of Ba^{2+} ions on the gating property of the membrane, the $BaCl_2$ concentration dependence of the permeability at 37°C was also investigated. As shown in **Figure 5(a)**, as the $BaCl_2$ concentration increases, the permeation flux decreases. Above 10 mM $BaCl_2$, the permeability decreases greatly. The tendency is again similar to that of the membrane prepared using the PE substrate. Furthermore, the filling ratio dependence of the permeability at the presence and absence of $BaCl_2$ at 37°C is shown in **Figure 6(a)**. The permeation flux decreases as the filling ratio increases, in both pure water and the 10 mM aqueous $BaCl_2$ solution. This indicates that pore size is reduced by increases in the amount of graft polymer, and coincides with the trend seen in the SEM image shown in Figure 3.

2.3 Analysis of pore size of the ion gating membrane with cylindrical straight pores

The ion gating membrane prepared with Cyclopore® should have straight pores with a narrow pore size distribution. Therefore, the pore diameter can be calculated from the permeation flux shown in Figures 4(a) to 6(a), using the Hagen–Poiseuille equation, which is valid for cylindrical straight pores. The permeation flux J in the Hagen–Poiseuille equation can be represented by Eq. (3).

$$J = \frac{\varepsilon \cdot \Delta P \cdot d^4}{32\mu \cdot L \cdot d_0^{\,2}} \tag{3}$$

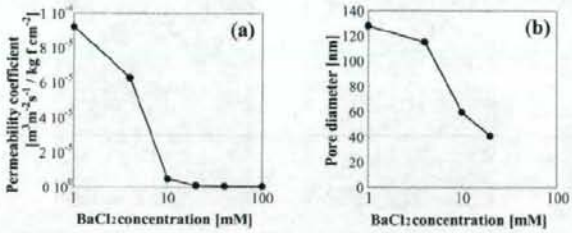

Fig. 5 $BaCl_2$ concentration dependence of membrane permeation properties (filling ratio 15.3%) at 37°C: (a) permeability coefficient; (b) pore diameter

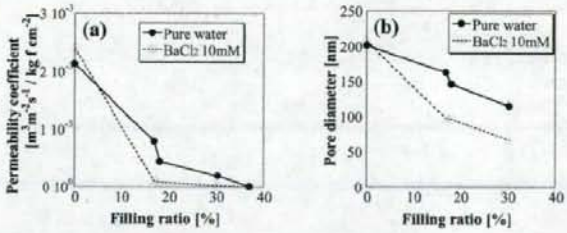

Fig. 6 Filling ratio dependence of membrane permeation properties for pure water and 10 mM aqueous $BaCl_2$ solution at 37°C: (a) permeability coefficient; (b) pore diameter

where, d [m] and d_0 [m] represent the pore diameter of the grafted and nongrafted membranes, respectively. L [m] and ε [—] are the thickness and porosity of the substrate. The permeation flux has a fourth power dependency on pore diameter, because the pore number density is always constant. We note that at low permeabilities, the relationship between permeability and pore size is more complex, given that the pore sizes will be less uniform because the distribution of the degree of polymerization and the fluctuation of polymer dimension may not satisfy the conditions of Eq. (3). Thus, we avoided the application of the equation at low permeabilities. The pore diameters derived from the permeation fluxes using the Hagen–Poiseuille equation are shown in **Figures 4(b)** to **6(b)**.

The validity of the evaluation is confirmed since the pore diameter calculated for the nongrafted membrane in Figure 6(b) is equal to 200 nm, which is the same as the nominal value of the Cyclopore® substrate used. Therefore, the pore size on the membrane can be calculated with this methodology. The dimensions of the grafted ion-responsive polymer can be evaluated using the pore diameters of the grafted and nongrafted membranes. We can observe large dimensional changes of the ion-responsive grafted polymer in response to temperature and $BaCl_2$ concentration in every figure. In Figure 6(b) in particular, the dimensional change is more than 3-fold at relatively low filling ratios. Our methodology and this information will contribute to the applications and designs of the molecular recognition ion gating membranes.

Conclusions

A molecular recognition ion gating membrane having cylindrical straight pores was developed by grafting an ion-responsive polymer onto the pore surface of a polycarbonate track-etched membrane substrate. Successful preparation of the membrane was confirmed by its weight change, FT–IR, and SEM images. The permeation flux of pure water and an aqueous $BaCl_2$ solution through the membrane was measured, and the gating properties of the membrane were investigated and confirmed to be similar to those of membranes prepared with a PE porous substrate. The information about pore sizes of the ion gating membrane was obtained using the Hagen–Poiseuille equation. Our analysis of the grafted ion-responsive polymer size showed a polymer's large dimensional change in response to temperature and specific ion concentration.

Literature Cited

Friebe, A. and M. Ulbricht; "Controlled Pore Functionalization of Poly(Ethylene Terephthalate) Track-Etched Membranes via Surface-Initiated Atom Transfer Radical Polymerization," *Langmuir*, **23**, 10318–10322 (2007)

Ito, T., T. Hioki, T. Yamaguchi, T. Shinbo, S.-I. Nakao and S. Kimura; "Development of a Molecular Recognition Ion Gating Membrane

and Estimation of Its Pore Size Control," *J. Amer. Chem. Soc.*, **124**, 7840–7846 (2002)

Irie, M., Y. Misumi and T. Tanaka; "Stimuli-Responsive Polymers—Chemical-Induced Reversible Phase-Separation of an Aqueous-Solution of Poly(*N*-Isopropylacrylamide) with Pendent Crown-Ether Groups," *Polymer*, **34**, 4531–4535 (1993)

Rui, X., L.-Y. Chu, W.-M. Chen, W. Xiao, H.-D. Wang and J. B. Qu; "Characterization of Microstructure of Poly(*N*-Isopropylacrylamide)-Grafted Polycarbonate Track-Etched Membranes Prepared by Plasma-Graft Pore-Filling Polymerization," *J. Membr. Sci.*, **258**, 157–166 (2005)

Ungaro, R., E. B. Haj and J. Smid; "Substituent Effects on Stability of Cation Complexes of 4′-Substituted Monobenzo Crown Ethers," *J. Amer. Chem. Soc.*, **98**, 5198–5202 (1976)

Yagi, K., J. A. Ruitz, M. C. Sanchez and C. Guerrero; "Cation Binding-Properties of Polymethacrylamide Derivatives of Crown Ethers," *Macromol. Chem. Rapid Commun.*, **1**, 263–268 (1980)

Yamaguchi, T., S.-I. Nakao and S. Kimura; "Plasma-Graft Filling Polymerization—Preparation of a New Type of Pervaporation Membrane for Organic Liquid Mixtures," *Macromolecules*, **24**, 5522–5527 (1991)

Yamaguchi, T., S.-I. Nakao and S. Kimura; "Evidence and Mechanisms of Filling Polymerization by Plasma-Induced Graft Polymerization," *J. Polym. Sci. Part A: Polym. Chem.*, **34**, 1203–1208 (1996)

Yamaguchi, T., T. Ito, T. Sato, T. Shinbo and S. I. Nakao; "Response Mechanism of a Molecular Recognition Ion Gating Membrane," *J. Amer. Chem. Soc.*, **121**, 4078–4079 (1999)

Journal of Chemical Engineering of Japan, Vol. 42, No. 2, pp. 86–94, 2009 **Research Paper**

A New Free Volume Theory Based on Microscopic Concept of Molecular Collisions for Penetrant Self-Diffusivity in Polymers

Hidenori OHASHI, Taichi ITO and Takeo YAMAGUCHI
Chemical Resources Laboratory, Tokyo Institute of Technology, R1-17, 4259, Nagatsuta-cho, Midori-ku, Yokohama-shi, Kanagawa 226-8503, Japan

Keywords: Self-Diffusivity in Polymer, Free Volume Theory, Molecular Collisions, Quantum Chemical Calculation

A new free volume theory, which we named "shell-like free volume" theory, is developed for penetrant diffusivity in polymers by introducing microscopic concept of molecular collisions. Shell-like free volume is defined as the ambient free space of the penetrant molecule; it is consistent with the notion of molecular collisions, which is the microscopic origin of molecular diffusion. The microscopic notion can give physical meaning to all the parameters in the theory, and the parameters can be evaluated using the only pure-component parameters: the experimental viscosity of the solvent, the viscoelasticity of the polymer, and the molecular surface area estimated from the chemical structure using the semiempirical quantum chemical calculation. The predictive ability of the shell-like free volume theory is good for self-diffusivities of molecules with shapes from spherical to chain-like in polymer solutions over wide ranges of temperature and concentration.

Introduction

Molecular diffusivity is one of the most important dynamic physical properties to control device characteristics because it governs molecular transport in many processes and devices. In particular, penetrant molecular diffusivity through polymer materials is important in such applications as separation membranes (Yamaguchi *et al.*, 1991; Park and Paul, 1997; Merkel *et al.*, 2000; Ho and Poddar, 2001), cast-drying polymer coating processes (Wong *et al.*, 2005), and polymerization processes (Russell *et al.*, 1993; Tefera *et al.*, 1997). Practical use of the diffusivity can greatly facilitate device designs; however, one difficulty is that the dynamic property is a mixing property, which has a large number of combinations between constituents, polymers and diffusing molecules. Therefore, the molecular diffusivity in a polymer is desired to be estimated using only pure-component physical properties having a much smaller number. In order to accomplish the requirement and better expression of the transport property, a number of theoretical investigations including the friction (Cukier, 1984; Phillies, 1989), obstruction (Mackie and Meares, 1955; Ogston *et al.*, 1973), molecular (Pace and Datyner, 1979a, 1979b; Kloczkowski and Mark, 1989), and free volume models (Fujita, 1961; Vrentas and Duda, 1977a, 1977b) have been proposed (Muhr and Blashard, 1982; Tirrell, 1984; Masaro and Zhu, 1999) up until now.

In the present investigation, we develop a new model based on free volume theory (Doolittle, 1951; Doolittle and Doolittle, 1957). The well-defined physical image of free volume theory is that it is only when a free volume hole of sufficient size opens up next to a penetrant molecule that the molecule can jump into the hole and diffusion can occur. It was formulated by Cohen and Turnbull (1959) and other researchers (Liu *et al.*, 2002), and the notion has been widely extended to penetrant diffusion in polymer systems (Fujita, 1961; Vrentas and Duda, 1977a, 1977b; Paul, 1983). In these theories, the idea that both polymers and solvents contribute to the free volume of the system is highly successful, especially in the Vrentas–Duda model (Vrentas *et al.*, 1996; Vrentas and Vrentas, 1998) and the Cohen–Turnbull model (von Meerwall *et al.*, 1998, 1999, 2007). The Vrentas–Duda model has been extensively studied to express the temperature, concentration, and molecular shape dependency of self-diffusivity of various penetrants in polymers, by introducing the notion of a polymer jumping unit and the idea that asymmetric molecular shapes influence the free volume distribution (Vrentas and Duda, 1977a; Vrentas *et al.*, 1996). The Cohen–Turnbull model, extended by von Meerwall *et al.* (1998, 1999, 2007), can accurately express the self-diffusivity of *n*-alkanes and polyethylene in their binary systems over wide temperature and molecular weight ranges, by introducing such concepts as molecular chain end effects, polymer entanglement, and

Received on May 29, 2008; accepted on October 15, 2008.
Correspondence concerning this article should be addressed to T. Yamaguchi (E-mail address: yamag@res.titech.ac.jp).

constraint release. These theoretical successes prompted us to use the sophisticated idea of free volume contribution in the present study.

Reconsidering the molecular diffusion phenomenon from the microscopic viewpoint, it is evident that molecular random walk movement originates in molecular collisions with adjacent molecules. From this standpoint, diffusion in simple systems has been described by collision-based models (Lamm, 1954; Dullien, 1963; Vanbeije and Ernst, 1973; Dymond, 1974; Atkins, 1990). In fact, molecular collisions are also an important feature of molecular diffusion in polymer-containing systems. If the microscopic concept of molecular collision is introduced into the diffusion model for polymeric systems, it can contribute to a sophisticated model that can describe molecular diffusivity in polymers based on the microscopically fundamental notion, but no such model has been developed. In the present study, we suggest a novel microscopic notion named "shell-like free volume" by reexamining microscopic molecular collisions, and introduce the concept into the fundamental equation of free volume theory (Cohen and Turnbull, 1959; Liu *et al*., 2002). Furthermore, the introduction of the microscopic concept finally enables estimation of the molecular diffusivity in a polymer as a mixing property, by using only pure-component physical properties. Then, by comparing experimental and calculated self-diffusivities of solvent molecules in polymers, the validity of the developed model is investigated.

1. Theory

1.1 A novel concept and definition of shell-like free volume

Molecular collisions create free space around a penetrant molecule, and only the contacting space is accessible for penetrant molecular motion, because a molecule drifts by colliding with adjacent molecules. In the present study, based on this microscopic idea, we developed a new concept, "shell-like free volume" around a molecule, as the amount of mean free space contacting the molecule (**Figure 1**). This shell-like free volume, referred to as D_s [cm³/molecule], is taken as the free volume per molecule in the free volume basic equation, and the following formula for molecular diffusivity D_s [cm²/s] is obtained.

$$D_s = D_0 \exp\left(-v^*/v_{f,slfv}\right) \tag{1}$$

where, D_s [cm²/s] is a preexponential factor, and v^* [cm³/molecule] is the critical molecular volume, which is the required space for a molecular diffusive jump. Usually, v^* is regarded as the volume occupied by a penetrant molecule at 0 K (Haward, 1970). The shell-like free volume $v_{f,SLFV}$ can be calculated as the product of penetrant molecular surface area s_i [Å²/molecule] (the unit is equal to 6.023×10^7 cm²/mol in SI units and for the facilitation of actual calculation, the SI unit will be used hereafter) and free volume thickness δ [Å] (the unit is equal to 1×10^{-8} cm and the SI units will be used hereafter). The simple physical meaning of the parameter $v_{f,SLFV}$ is that as the space around the molecule increases, it becomes easier for the molecule to move. This image seems to agree reasonably well with actual images of molecular movement. Here, we note that our first target is the systems composed of nonpolar substances in which there is no strong interaction between the molecules that reduce molecular collisions.

Fig. 1 Schematic illustration of "shell-like free volume" around a molecule

1.2 Calculation of shell-like free volume

Penetrant and polymer each have their own free volume $V_{f,i}/\gamma$ [cm³/g] of component i (i = 1, 2, where the subscript 1 represents penetrant, such as solvent, and 2 represents polymer hereafter). The amount of free volume $V_{f,i}/\gamma$ is an inherent property of each substance, and it can be estimated directly using the substance's dynamic physical property, such as the rheological property of the pure component, as shown later in Section 2.4. The free volume thickness of each pure-component, δ_i [cm], can be calculated by dividing the inherent free volume amount [cm³/g] by the molecular surface area [cm²/g] (**Figure 2**).

$$\delta_i = \left(V_{f,i}/\gamma\right)/\left(s_i N_A/M_i\right) \tag{2}$$

where, s_i [cm²/mol] and M_i [g/mol] represent the molecular surface area and molecular weight of component i, respectively, and N_A is Avogadro's number.

Using information about molecular surface area and free volume thickness, the shell-like free volume can be calculated. A penetrant molecule contacts with other molecules on its surface, and the contacting proportion is equal to a surface area fraction σ_i [cm²/cm²], expressed as shown in Eq. (3).

$$\sigma_i = \frac{\text{Summation of molecular surface area of component } i}{\text{Summation of surface area of all molecules included in system}} = \frac{\omega_i (s_i/M_i)}{\sum_j \omega_j (s_j/M_j)} \tag{3}$$

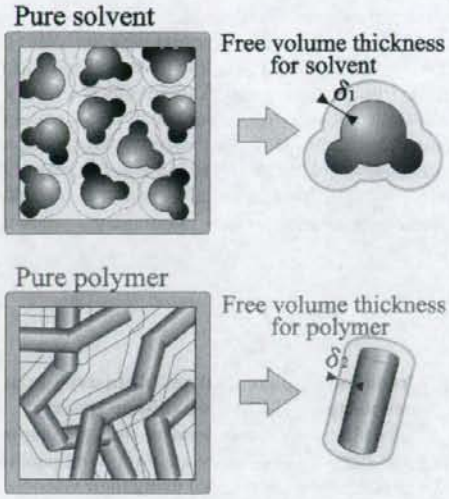

Fig. 2 Schematic illustration of free volume thickness of solvent and polymer; the free volume thickness of each component can be calculated by dividing the pure-component free volume $V_{f,i}/\gamma$ by its molecular surface area $s_i N_A/M_i$

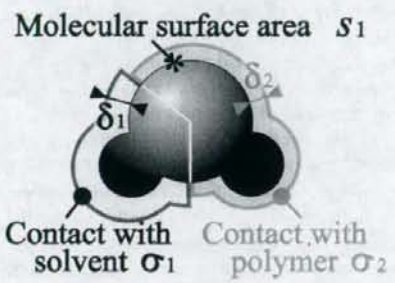

Fig. 3 The shell-like free volume can be calculated as the product of molecular surface area s_1 and free volume thickness; a penetrant molecule contacts the solvent over a surface area fraction σ_1 and contacts the polymer over the fraction σ_2; the free volume thickness assigned by the solvent is δ_1, and that assigned by the polymer is δ_2; the shell-like free volume $v_{f,SLFV}$ is therefore $s_1(\sigma_1\delta_1 + \sigma_2\delta_2)$

where, ω_i [g/g] represents the weight fraction of component i.

It is reasonable that the free volume thickness of each component δ_i should be assigned to the penetrant molecule in proportion to its corresponding surface area fraction σ_i (**Figure 3**) and the shell-like free volume can be calculated as shown in Eq. (4).

$$v_{f,SLFV} = s_1 \sum_i \sigma_i \delta_i \tag{4}$$

Thus, by combining Eqs. (1) to (4), the penetrant self-diffusivity in our model is shown by Eq. (5).

$$\begin{aligned} D_{s1} &= D_0 \exp\left(-v^*/v_{f,SLFV}\right) \\ &= D_0 \exp\left\{-\hat{V}_1^* M_1/N_A \Big/ s_1 \sum_i \left[\frac{\omega_i s_i/M_i}{\sum_j \omega_j (s_j/M_j)} \cdot \frac{(V_{f,i}/\gamma)}{s_i N_A M_i}\right]\right\} \\ &= D_0 \exp\left[-\frac{\hat{V}_1^* M_1 \sum_j \omega_j (s_j/M_j)}{s_1 \cdot \sum_i \omega_i (V_{f,i}/\gamma)}\right] \end{aligned} \tag{5}$$

where, $\hat{V}_1^*$ [cm^3/g] is the critical volume of component i and can be calculated as $\hat{V}_1^* = v_1^* N_A/M_1$. In Eq. (5), $\sum\omega_i(V_{f,i}/\gamma)$ is the total free volume contained in the mixed system $V_{f,sys}/\gamma$ [cm^3/g] (subscript i is used for the summation of free volume), and $N_A\sum\omega_j(s_j/M_j)$ is the total surface area of all molecules contained in the system S_{sys} [cm^2/g] (subscript j is used for the summation of molecular surface area); thus, Eq. (5) can be rewritten as Eq. (6).

$$D_{s1} = D_0 \exp\left[-\frac{\hat{V}_1^* M_1/N_A}{s_1 \cdot \left(V_{f,sys}/\gamma S_{sys}\right)}\right] \tag{6}$$

Equations (5) and (6) are the formulas for "shell-like free volume" theory.

To make a calculation using Eq. (5), values of the molecular surface area s_i and the free volume amount $V_{f,i}/\gamma$ of component i are required as model parameters. Estimation of the parameters is shown in the following sections.

1.3 Calculation of molecular surface area using a semiempirical quantum chemical calculation

A semiempirical quantum chemical calculation was used to estimate the molecular surface area of pure solvents and pure polymers from their chemical structures. A computer-aided chemistry modeling program, CAChe (Fujitsu Ltd.), was used for the whole calculation.

The computation procedure for the molecular surface area is as follows. First, one molecule was produced on the molecular structure console of CAChe. The constructed molecular structure was optimized by using the molecular mechanics calculation, and was then optimized using a semiempirical quantum chemical calculation; finally, the isoelectric surface and its surface area were calculated using a semiempirical calculation. The PM3 method was chosen as the semiempirical quantum chemical calculation method (Stewart, 1989; Dewar *et al.*, 1990), and an electron density of 0.0020 a.u. (1 a.u. is defined as 6.748 e/Å^3)